Monthly Notices
of the
ROYAL ASTRONOMICAL SOCIETY

Mon. Not. R. Astron. Soc. **423,** 2879–2892 (2012) doi:10.1111/j.1365-2966.2012.21098.x

Probing the time variability of five Fe low broad absorption-line quasars⋆

M. Vivek,[1]† R. Srianand,[2] P. Petitjean,[3] P. Noterdaeme,[3] V. Mohan,[2] A. Mahabal[4] and V. C. Kuriakose[1]

[1]*Department of Physics, Cochin University of Science and Technology, Kochi 682022, India*
[2]*Inter-University Centre for Astronomy and Astrophysics, Pune 410007, India*
[3]*UPMC-CNRS, UMR7095, Institut d'Astrophysique de Paris, 98bis Boulevard Arago, 75014 Paris, France*
[4]*Caltech, MC 249-17, Pasadena, CA 91125, USA*

Accepted 2012 April 12. Received 2012 April 6; in original form 2012 January 10

ABSTRACT

We study the time variability of five Fe low-ionization broad absorption line (FeLoBAL) QSOs using repeated spectroscopic observations with the 2-m telescope at IUCAA Girawali Observatory (IGO) spanning an interval of up to 10 years. We report a dramatic variation in the Al III and Fe III fine-structure lines in the spectra of SDSS J221511.93−004549.9 ($z_{\rm em} \sim 1.478$). However, there is no such strong variability shown by the C IV absorption. This source is known to be unusual with (i) the continuum emission dominated by Fe emission lines, (ii) Fe III absorption being stronger than Fe II and (iii) the apparent ratio of Fe III UV 48 to Fe III UV 34 absorption suggesting an inverted population ratio. This is the first reported detection of time variability in the Fe III fine-structure lines in QSO spectra. There is a strong reduction in the absorption strength of these lines between 2000 and 2008. Using the template-fitting techniques, we show that the apparent inversion of the strength of ultraviolet lines could be related to the complex spectral energy distribution of this QSO. The observed variability can be related to a change in the ionization state of the gas or due to the transverse motion of this absorbing gas. The shortest variability time-scale of Al III line gives a lower limit on the electron density of the absorbing gas as $n_{\rm e} \geq 1.1 \times 10^4\,{\rm cm}^{-3}$. The remaining four FeLoBALs do not show any changes beyond the measurement uncertainties either in optical depth or in the velocity structure. We present the long-term photometric light curve for all of our sources. Among them only SDSS J221511.93−004549.9 shows significant ($\geq$0.2 mag) variability.

Key words: galaxies: active – quasars: absorption lines – quasars: general.

1 INTRODUCTION

Broad absorption line (BAL) quasars form ∼20–40 per cent of the QSO population (Hewett & Foltz 2003; Reichard et al. 2003; Trump et al. 2006; Dai, Shankar & Sivakoff 2008; Allen et al. 2011; Stalin, Srianand & Petitjean 2011) and are characterized by the presence of broad absorption lines spreading over 5000–50 000 km s^{-1} (Green et al. 2001). BAL QSOs are further classified into three subgroups based on the material producing the BAL troughs. High-ionization BALs (HiBALs) contain strong, broad absorption troughs of highly ionized species such as C IV, O VI and N V and are typically identified through the presence of C IV absorption troughs. Low-ionization BALs (LoBALs) contain absorption from low-ionization species such as Mg II, Al II or Al III in addition to the standard absorption lines seen in HiBALs. The LoBALs comprise about 15 per cent of the BAL population. A small subset of LoBALs with the excited-state Fe II or Fe III absorption are termed as FeLoBALs (Wampler, Chugai & Petitjean 1995). Only 13 per cent of the LoBALs (i.e. 1 per cent of the total BAL population) are FeLoBALs. The catalogue of BAL quasars in Sloan Digital Sky Survey Data Release 3 (SDSS DR3) by Trump et al. (2006) has 138 FeLoBALs. As these QSOs are very rare, they are not a well-studied population of BAL QSOs.

FeLoBALs are also found to be the most reddened ones among BAL quasars (Reichard et al. 2003). The FeLoBALs are found to be extremely infrared (IR) luminous (Farrah et al. 2007), with IR

⋆ This paper uses archival data based on observations carried out at the European Southern Observatory (ESO) under programmes 267.B-5698 and 71.B-0121.

†E-mail: vivekm@iucaa.ernet.in

luminosities comparable to those of ultraluminous infrared galaxies (ULIRGs). Hence, the FeLoBAL phenomenon could be considered as a transition stage in a ULIRG when the starburst is at or near its end, and the central QSO is starting to throw off its dust cocoon (Voit, Weymann & Korista 1993; Farrah et al. 2007). This scenario strongly favours the theory of the BAL QSO to be an evolutionary stage in a quasar lifetime, rather than an orientational effect. The C IV BALs are reported to be located at a distance of $\lesssim$1 pc (e.g. Capellupo et al. 2011). However, the ionization parameter and density estimates of some of the FeLoBALs are consistent with the absorbing gas at $\geq$1 kpc from the continuum source (Korista et al. 2008; Moe et al. 2009; Bautista et al. 2010; Dunn et al. 2010; Faucher-Giguère, Quataert & Murray 2012). This together with very small inferred thickness of the cloud prompted Faucher-Giguère et al. to suggest that FeLoBALs must be formed in situ at large radii through an interaction of the QSO blast wave in the interstellar medium (ISM) of the host galaxy. In this scenario the time evolution of the post-shock gas will be seen as the absorption-line variability.

Repeated BAL monitoring studies could greatly help us in understanding the location and physical conditions in the absorbing gas and the physical mechanisms responsible for quasar outflows. Time variability of Si IV and C IV BALs in individual sources has been reported in several BAL QSOs: Q1303+308 (Foltz et al. 1987), Q1413+113 (Turnshek et al. 1988), Q1246−057 (Smith & Penston 1988), UM 232 (Barlow, Junkkarinen & Burbidge 1989), QSO CSO 203 (Barlow et al. 1992), Tol 1037−270 (Srianand & Petitjean 2001), J1054+0348 (Hamann et al. 2008) and FBQS J1408+3054 (Hall et al. 2011). Lundgren et al. (2007) have reported significant time variability among a sample of 36 C IV BALs on rest-frame time-scales shorter than 1 year. Gibson et al. (2008) also report a similar result in a sample of 13 quasars ($1.7 \leq z \leq 2.8$) over 3–6 (rest frame) years. Gibson et al. (2010) investigated the C IV BAL variability of 14 sources at redshifts >2.1 and report complex variations in the sample. In these cases, changes in the rest equivalent width of absorption lines are used as an indicator of variability. This requires continuum fitting that is in general ambiguous in the case of BAL QSOs. Capellupo et al. (2011) have studied the C IV BAL variability in 34 luminous QSOs over short (4–9 months) and long (3.8–7.7 years) time-scales. They used flux differences between two epoch data at the absorption trough to quantify the variability. However, no such studies are reported for the LoBALs and in particular there is no case reported showing the variability of absorption lines originating from excited fine-structure levels in the case of BAL QSOs.

QSO feedback plays an important role in the evolution of the host galaxy. If FeLoBALs represent a transition state (or post-shock ISM gas) as discussed above, then repeated spectroscopic monitoring of these sources will shed light on the evolutionary scenarios of QSOs. In this paper, we report the nature of time variability in a sample of five FeLoBAL quasars. This is a subsample of our ongoing spectroscopic monitoring campaign on time variability of absorption lines in a sample of 27 LoBAL quasars. Three of the sources, SDSS J030000.57+004828.0 (hereafter SDSS J0300+0048), SDSS J031856.62−060037.7 (hereafter SDSS J0318−0600) and SDSS J221511.93−004549.9 (hereafter SDSS J2215−0045), are from the 23 SDSS Early Data Release (EDR)-listed quasars identified by Hall et al. (2002) as BAL quasars exhibiting various unusual properties. The other two sources are SDSS J083522.77+424258.3 (hereafter SDSS J0835+4242) and SDSS J084044.41+363327.8 (hereafter SDSS J0840+3633).

This paper is arranged as follows. In Sections 2 we provide details of observation and data reduction. Discussions on individual sources in our sample are presented in Sections 3. Implications of the variability seen in SDSS J2215−0045 are presented in Sections 4 and the main results are summarized in Sections 5.

2 OBSERVATION AND DATA REDUCTION

Most of the new observations presented here were carried out using the 2-m telescope at IUCAA Girawali Observatory (IGO). The spectra were obtained using the IUCAA Faint Object Spectrograph (IFOSC). The detailed log of these observations together with that of the archival SDSS data and the data from the literature are given in Table 1. Spectra were originally obtained mainly using three grisms, grism 1, grism 7 and grism 8 of the IFOSC in combination with a 1.5-arcsec slit. This combination has a wavelength coverage of 3270–6160, 3800–6840 and 5800–8350 Å for the above three grisms, respectively. Typically the observations were split into exposures of 45 min. All the raw frames were processed using standard IRAF[1] tasks. One-dimensional spectra were extracted from the frames using the 'DOSLIT' task in IRAF. We opted for the variance-weighted extraction as compared to the normal one. Wavelength calibrations were done using standard helium neon lamp spectra and flux calibrations were done using a standard star spectrum observed on the same night. Air-to-vacuum conversion was applied before adding the spectra. Individual spectra were combined using $1/\sigma^2$ weighting in each pixel after scaling the overall individual spectra to a common flux level within a sliding window. The error spectrum was computed taking into account proper error propagation during the combining process.

Our IGO spectrum of J2215−0045 taken in 2008 has shown dramatic variability as compared to the archival SDSS spectrum. To confirm this trend we obtained a moderate resolution echellete spectrum of the source using the Magellan Echellette (MagE) Spectrograph mounted on the Clay (Magellan II) telescope. We used a 1-arcsec slit and 1×1 binning for our observations. The available grating in combination with the 1-arcsec slit gives a resolution of $R = 4200$ and wavelength coverage of 3000–10 000 Å. Spectrophotometric standards were also observed for flux calibrations. MagE data were reduced using the MagE Spectral Extractor (MASE) pipeline (Bochanski et al. 2009). MASE is an IDL-based pipeline containing a graphic user interface for reducing the MagE data. VLT-UVES data (programme ID: 267.B-5698) taken on 2001 are available for this source in the VLT archive. We also used the VLT-FORS1 data (programme ID: 71.B-0121) obtained for this source in 2003 and made available to us by Dr DiPompeo (DiPompeo, Brotherton & De Breuck 2011).

In Fig. 1, we plot for all our sources Johnson's V magnitude from the Catalina Real-Time Transient Survey (CRTS; Drake et al. 2009) as described below. CRTS operates with an unfiltered set-up and the resulting magnitudes are converted to V magnitudes using the transformation equation $V = V_{\rm ins} + a(v) + b(v)(B - V)$, where, $V_{\rm ins}$ is the observed open magnitude, $a(v)$ and $b(v)$ are the zero-point and the slope, respectively. The zero-point and the slope are obtained from three or more comparison stars in the same field with the zero-point typically being of the order of 0.08. CRTS provides four such

[1] IRAF is distributed by the National Optical Astronomy Observatories, which are operated by the Association of Universities for Research in Astronomy, Inc., under cooperative agreement with the National Science Foundation.

Table 1. Log of observations.

QSO	Instrument	Date	MJD	Exposure time (min)	λ coverage (Å)	Resolution (km s^{-1})	S/N[a]
	SDSS	29-09-2000	51816	45×1	3800–9200	150	44
	SDSS	29-11-2000	51877	50×1	3800–9200	150	40
J0300+0048	SDSS	23-10-2001	52205	45×1	3800–9200	150	33
	IGO/IFOSC 7	12-12-2007	54446	35×2	3800–6840	310	5
	IGO/IFOSC 7	27-12-2008	54817	45×8	3800–6840	310	54
	SDSS	15-01-2001	51924	80×1	3800–9200	150	27
	IGO/IFOSC 8	14-12-2007	54448	45×3	5800–8350	240	10
	IGO/IFOSC 7	09-01-2008	54474	45×3	3800–6840	310	23
J0318−0600	IGO/IFOSC 8	27-11-2008	54797	45×3	5800–8350	240	21
	IGO/IFOSC 7	31-01-2009	54862	45×4	3800–6840	310	19
	IGO/IFOSC 8	23-12-2009	55188	45×4	5800–8350	240	19
	IGO/IFOSC 7	24-12-2009	55189	45×4	3800–6840	310	17
	SDSS	19-11-2001	52232	48×1	3800–9200	150	26
J0835+4242	IGO/IFORS 1	14-12-2007	54448	45×3	3270–6160	370	9
	IGO/IFOSC 7	05-12-2008	54805	45×3	3800–6840	310	21
	IGO/IFOSC 7	21-01-2010	55217	45×3	3800–6840	310	29
	SDSS	15-02-2002	52320	50×1	3800–9200	150	40
	IGO/IFOSC 7	20-12-2006	54089	45×3	3800–6840	310	8
J0840+3633	IGO/IFOSC 7	12-12-2007	54446	45×3	3800–6840	310	23
	IGO/IFOSC 7	07-12-2008	54807	45×4	3800–6840	310	26
	IGO/IFOSC 7	17-12-2009	55182	45×6	3800–6840	310	50
	SDSS	04-09-2000	51804	53×1	3800–9200	150	41
	VLT/UVES	11-08-2001	52145	60×2	3000–11 000	7.3	43
	VLT/FORS 1	20-09-2003	52902	5×1	3300–11 000	250	62
	IGO/IFOSC 7	31-10-2008	54783	45×3	3800–6840	310	30
	IGO/IFOSC 7	01-11-2008	54784	45×1	3800–6840	310	23
J2215−0045	IGO/IFOSC 8	01-11-2008	54784	45×4	5800–8350	240	39
	IGO/IFORS 1	02-01-2010	55211	45×1	3270–6160	370	11
	IGO/IFORS 1	04-01-2010	55213	45×3	3270–6160	370	15
	MagE	10-08-2010	55431	15×1	3100–10 000	70	16
	IGO/IFORS 7	14-12-2010	55557	45×2	3800–6840	310	7
	IGO/IFORS 7	15-12-2010	55558	45×1	3800–6840	310	9
	IGO/IFORS 7	18-12-2010	55561	45×2	3800–6840	310	11
	IGO/IFORS 1	12-12-2011	55920	45×3	3270–6160	370	14
	IGO/IFORS 1	14-12-2011	55922	45×4	3270–6160	370	17

[a]Signal-to-noise ratio calculated over the wavelength range 5800–6200 Å.

observations taken 10 min apart on a given night. For our light curves we have averaged these four points (or less if one or more of those coincided with bad areas) and plotted those against the modified Julian date (MJD). The data used in these light curves are taken between 2005 April and 2010 July. The dotted vertical lines show the epochs of our spectroscopic observations. For J2215−0045, we could get the photometric data since 2004. The first point in the light curve for this source is obtained using g and r magnitudes in the SDSS and the transformation equation given by Jester et al. (2005) for QSOs at $z \leq 2.1$. For the other three sources we did not transform the SDSS magnitudes to Johnson V magnitude as the g- and r-band fluxes are affected by strong broad absorption lines. For all the sources, we have overplotted the average magnitudes obtained for closely spaced observations. The period over which the magnitudes are averaged is shown by x-axis error bars.

From the light curves, it is clear that continuum variability is apparent in all the sources. However, continuum variability at the level of >0.2 mag is seen only in the case of J2215−0045. The source has brightened by 0.3 mag when we consider only the CRTS points. The brightening could be up to 0.5 mag when we also include the transformed SDSS magnitude.

3 NOTES ON INDIVIDUAL OBJECTS

In this section, we summarize the properties of individual absorbers in our sample and discuss our monitoring results.

3.1 SDSS J0300+0048

SDSS J0300+0048 ($z_{\rm em} = 0.8918$) is part of a binary QSO with SDSS J025959.69+004813.5 ($z_{\rm em} = 0.8923$), a non-BAL QSO at a projected separation of 19.8 arcsec. It is only the fourth QSO known to have a Ca II BAL trough. The outflow is blue shifted by 1650 km s^{-1} from the systemic redshift of the QSO. Hall et al. (2003) obtained the high-resolution UVES spectrum of this source and found that extremely broad Mg II, Fe II and its fine-structure line absorptions are also present along with the strong Ca II absorption. They also found that the lowest velocity BAL region has a strong

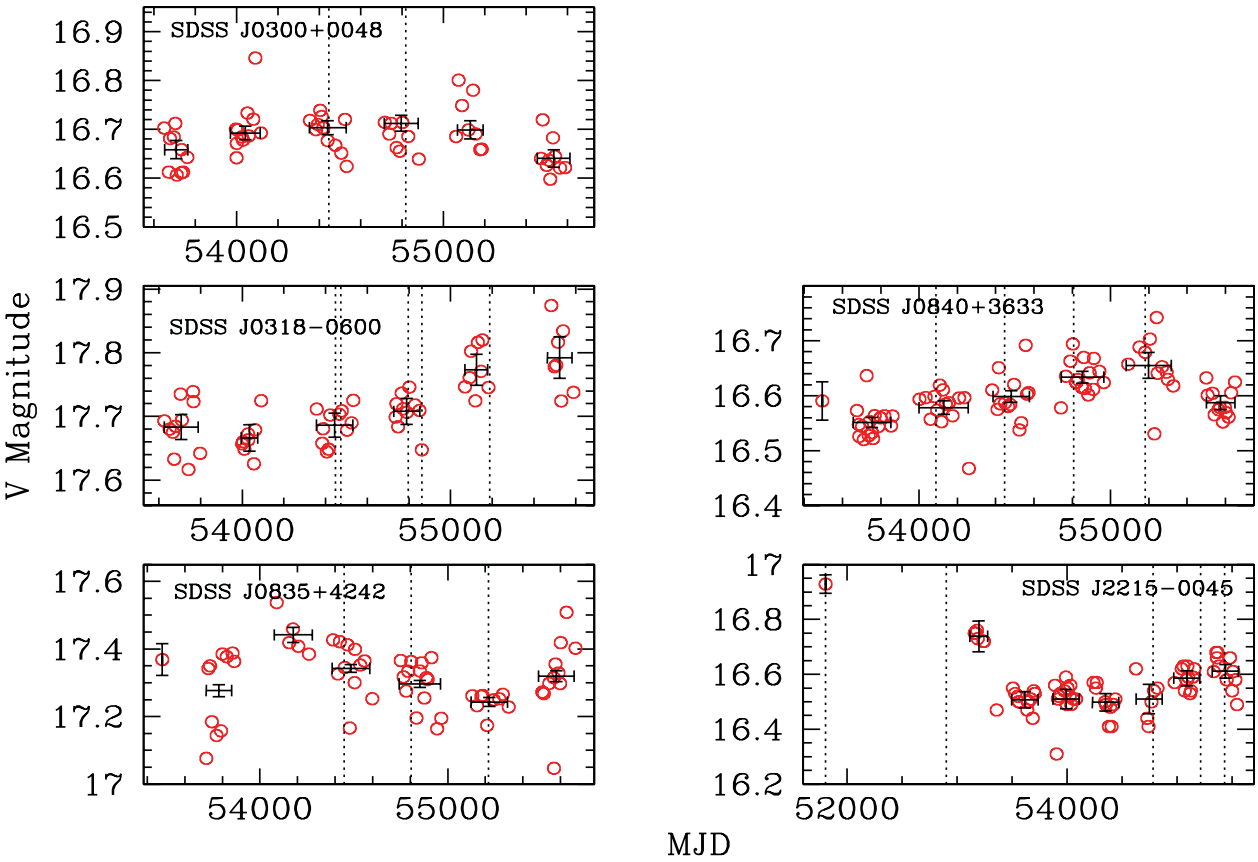

Figure 1. Light curves of five FeLoBAL quasars in the sample. The dotted vertical lines mark the epochs (MJDs) of spectroscopic observations. The average magnitudes obtained for closely spaced observations are overplotted as points with error bars for all sources. The *x*-axis error bars correspond to the time range over which the magnitudes are averaged.

Ca II absorption without a significant associated excited Fe II absorption, while the higher velocity excited Fe II absorption region has very little Ca II absorption. The reported Ca II, Mg II and Mg I column densities are very high and the corresponding gas phase metallicity is found to be 15 times the solar value. Comparing these large column densities to that of QSO J2359−1241, Hall et al. (2003) argued that this source must have a strong hydrogen ionization front where the Ca II exists outside the H I front. As the lowest ionization gas is found at lowest velocities, they explained the detached flow in SDSS J0300+0048 by the radiatively driven disc wind model by Murray & Chiang (1995). Apart from the BAL, there is a narrow associated absorption system detected by Ca II, Mg II, Mg I and Fe II lines at a redshift of $z_{\rm abs} = 0.8918$. Hall et al. (2003) have also suggested that the optical part of the QSO continuum is dominated by the Fe II and Fe III emission line blends. An important feature of this spectrum is that the flux values never return to the continuum values (as shown by Hall et al. 2003) shortwards of the rest wavelength 3000 Å ($\lambda_{\rm obs} \sim 5675$ Å). Also, emission bumps seen around the rest wavelength range 3000–3300 Å ($\lambda_{\rm obs} \sim 5675$–6240 Å) are consistent with them being dominated by Fe emission.

In Fig. 2 we compare different SDSS and IGO spectra with the reference SDSS spectrum observed on MJD 51877. The spectra are aligned by a simple scaling of the mean flux. The spectral ranges covered by absorption of different species are marked with horizontal lines in each panel. It is clear from Fig. 2 that there is additional absorption at the rest wavelength of $\lambda_{\rm obs} \sim 4950$ Å that cannot be accommodated by the Fe II UV 63 absorption. This could be due to an additional blue shifted Mg II component not identified by Hall et al. (2003). The corresponding Fe II UV 2 absorption can explain the absorption trough at $\lambda_{\rm obs} \sim 4950$ Å seen in Fig. 2. In the bottom of each panel we show the difference between the two spectra plotted in the upper part together with the associated errors estimated from the error spectra. If required, in order to take care of spectral slope differences, we have fitted a lower order polynomial to the difference spectra considering regions that are devoid of absorption lines. For all the sources, the spectra are smoothed by 5 pixels for better presentation. However, the unsmoothed spectra are used for obtaining the difference and ratio spectrum.

The two-epoch SDSS data and our IGO spectrum obtained in year 2007 (MJD 54446) are nearly consistent with the reference SDSS spectrum within measurement uncertainties. We do not find any significant deviations in the difference spectra at the locations of strong absorption lines. However, it must be remembered that Mg II and Fe II transitions are highly saturated. Therefore, we may not be able to detect small column density variations. However, part of the absorption by Fe II fine-structure transition UV 63 is unsaturated. So, if there is any variability we should have detected the same. From Fig. 2 it is clear that even this transition does not show any detectable variability.

However, the plot suggests some differences between the SDSS and IGO spectra obtained in 2008. This is evident from the fact that the feature around $\lambda_{\rm obs} \sim 4700$ Å is consistently stronger in the IGO spectrum. The difference spectrum is found to be consistently above zero over 200 pixels, suggesting an excess at the $>10\sigma$ level. As discussed before, this part of the spectrum never recovers to the expected continuum level and therefore is subject to some

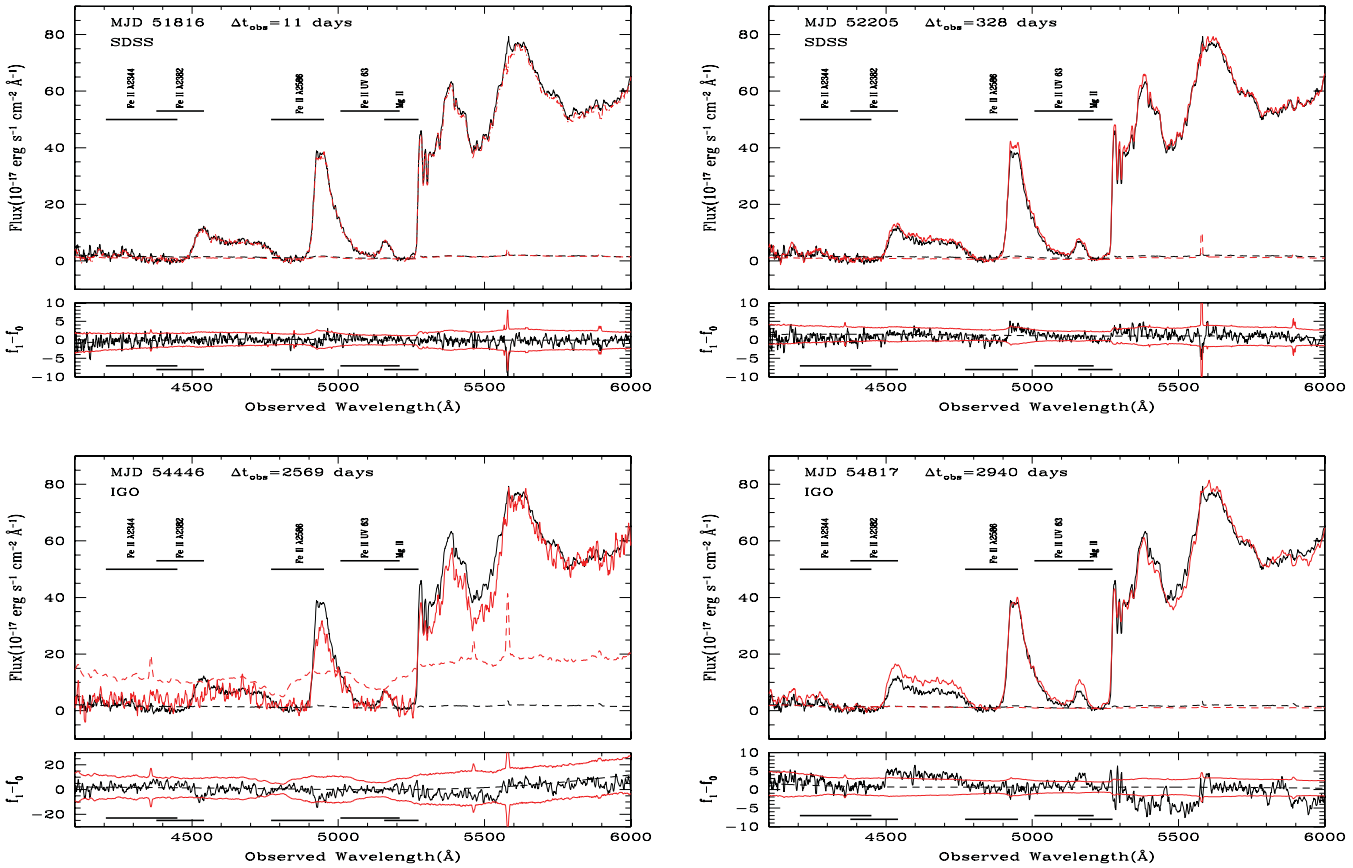

Figure 2. Spectra of SDSS J0300+0048 observed in SDSS (observed on MJD 51816 and 52205) and IGO (observed on MJD 54446 and 54817) (in red/grey) are overplotted with the reference SDSS spectrum (black) observed on MJD 51877. The flux scale applies to the reference SDSS spectrum and all other spectra are scaled in flux to match the reference spectrum. In each plot, the error spectra are also shown. The difference spectrum for the corresponding MJDs is plotted in the lower panel of each plot. 1σ error is plotted above and below the mean. The regions of absorption lines are marked with horizontal lines.

absorption. This could be the Fe II λ2600 absorption of the possible blue component discussed above. Similarly, we see significant deviation at $\lambda \sim 5500$ Å. The continuum emission in this region is dominated by Fe II and Mg II emission. Therefore, the variability is not related to absorption-line variability.

So, we conclude that a major part of BAL absorption lines of SDSS J0300+0048 that contains Fe II fine structure and Ca II (as identified by Hall & Hutsemèkers 2003) has not varied significantly over a time period of ∼4.2 years in the quasar rest frame. From Fig. 1, we note that on an average the V magnitude of this QSO remained the same within 0.05 mag over several years. Thus, the photoionization-induced variability is not expected as well. However, we report the possible variation of the bluest component. Future monitoring observations are needed to confirm the nature of the noted variability.

3.2 SDSS J0318−0600

SDSS J0318−0600 is a bright, reddened FeLoBAL of emission redshift $z_{\rm em} = 1.9669$. Bautista et al. (2010) and Dunn et al. (2010) studied the high-resolution VLT spectrum of this source and identified 11 absorption components spanning a velocity range of −7400 to −2800 km s^{-1} with the absorbing clouds fully covering the emitting regions of the background QSO. From photoionization models, they report super-solar abundances, an electron density of $10^{3.3\ \pm0.2}$ cm^{-3} and the distance from the emission source to the strongest component as 6 ± 3 kpc. The ratio of measured kinetic to bolometric luminosities is large enough to consider this outflow a significant contributor to the quasar feedback mechanism (Faucher-Giguère et al. 2012). The observed IGO spectra at various epochs are overplotted with the reference SDSS spectrum (MJD 51924) in Fig. 3. The BAL trough has multiple narrow components covering a large wavelength range. We identify four distinct components at $z_{\rm abs} = 1.895$, 1.911, 1.927 and 1.941 with the strongest component being at $z_{\rm abs} = 1.927$. The spectrum has well-defined absorption structures of Si IV, C IV, Al II, Al III, Mg II, Fe II and its excited states.

Individual components of C IV and Mg II lines are saturated (see fig. 3 of Dunn et al. 2010). As the line widths are close to our spectral resolution, we smoothed the SDSS spectrum to the IFOSC resolution for comparison. Some of the variations seen in the case of Fe II λ2600 and Fe II λ2383 are mainly due to atmospheric absorption that were not corrected in the IFOSC spectra. These regions of strong telluric absorption are marked in the spectra by crossed circles.

The prominent absorption components are labelled in Fig. 3 and the extent of the absorption is shown with horizontal lines. We note continuum shape differences between the IGO and SDSS spectra. To take care of this we fitted a smooth lower order polynomial to the difference spectrum avoiding the absorption-line regions and regions affected by telluric lines. It is clear from the bottom part of each panel that there is no significant deviation spread over the wavelength range covered by absorption in any of the cases.

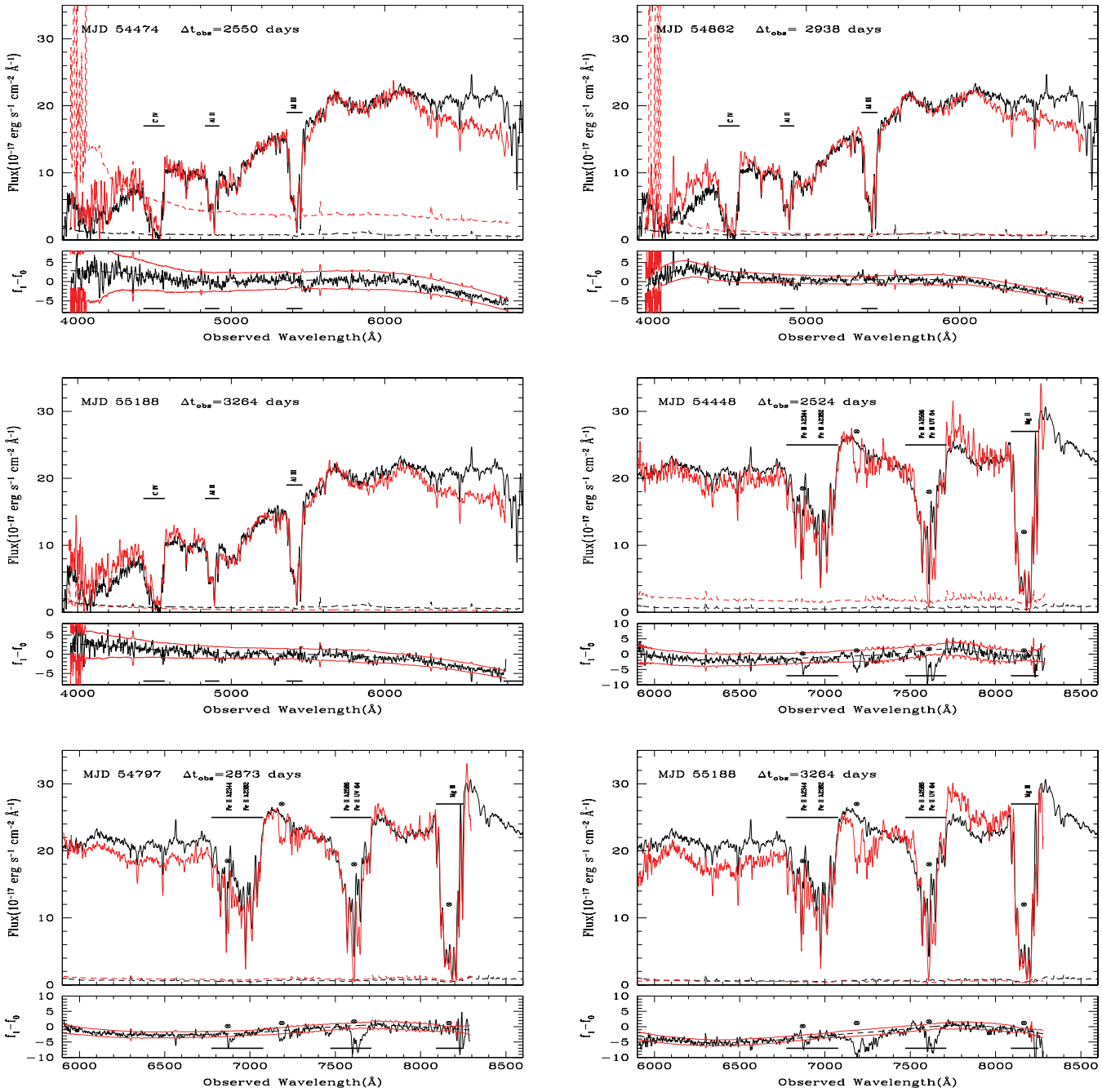

Figure 3. Spectra of SDSS J0318−0600 observed at different epochs at IGO (plotted in red/grey) are overplotted with the reference SDSS spectra (black). The flux scale applies to the reference SDSS spectrum and all other spectra are scaled to match the reference spectrum in continuum. In each plot, the error spectra are also shown. The difference spectra for the corresponding epoch together with the associated errors are plotted in the lower panel of each plot. The regions of absorption lines are marked with horizontal lines. The regions of strong telluric absorption are marked by crossed circles.

Strong deviations are seen only in regions where there is telluric contamination in our IFOSC spectrum.

Hence, we conclude that SDSS J0318−0600 shows no significant variability over a time-scale of 3 years in the quasar rest frame. The light curve presented in Fig. 1 suggests a smooth dimming of the QSO (by $\lesssim$0.1 mag). Our IGO spectra have slightly low continuum flux compared to the SDSS spectrum in the wavelength range 6000–7000 Å. This could be related either to the uncertainty related to extinction corrections or spectral variability of the QSO. However, this does not affect our conclusion regarding the absence of variability in the absorption lines.

3.3 SDSS J0835+4242

The redshift of this BAL QSO is $z_{\rm em} = 0.810$. Fig. 4 shows the comparison between the reference SDSS and IGO data for SDSS J0835+4242. IGO data acquired in the year 2010 (MJD 55217) have slightly lower resolution compared to the data taken in 2008

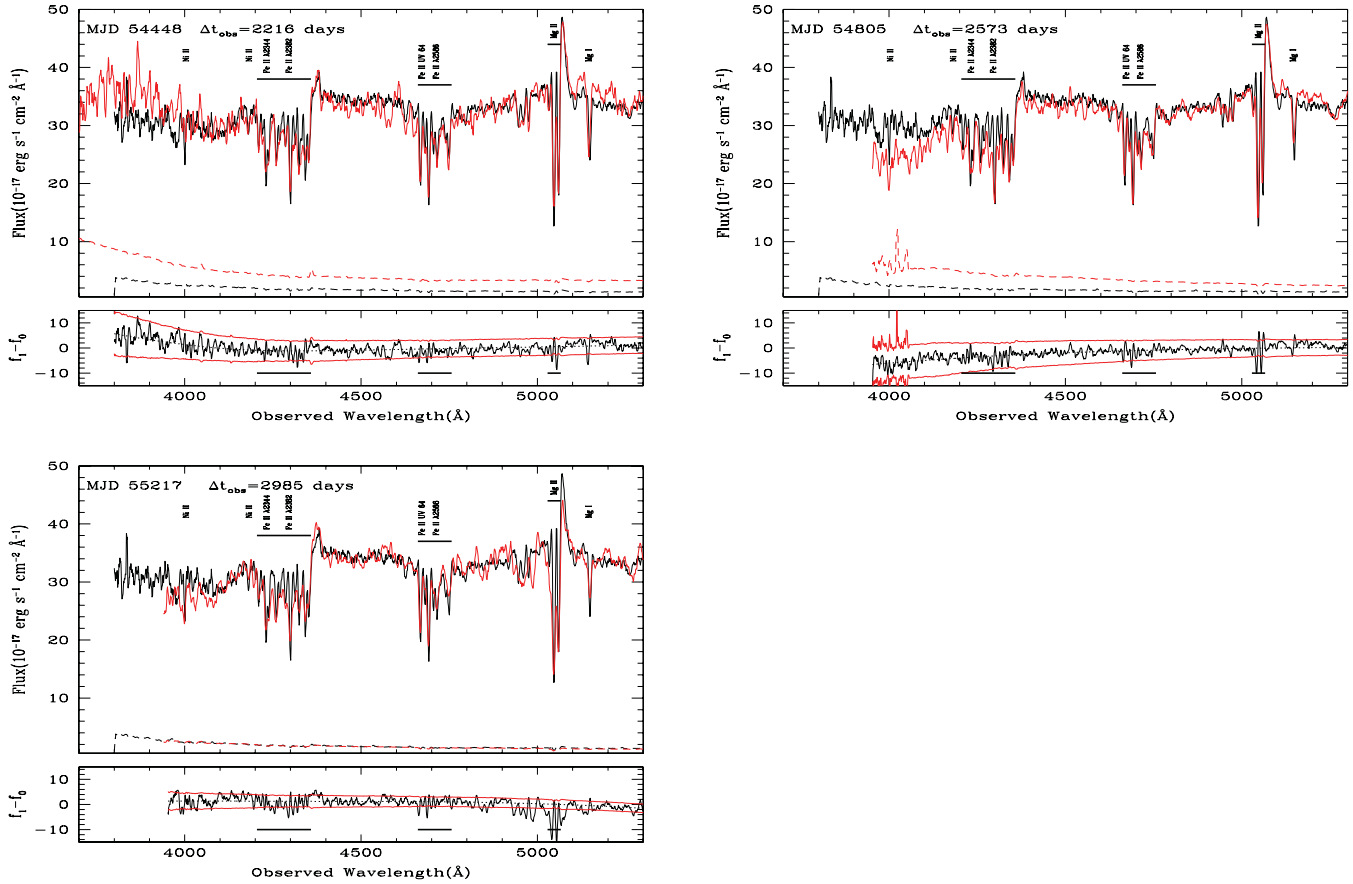

Figure 4. Spectra of SDSS J0835+4242 from IGO (red) epochs are overplotted with the reference SDSS spectra (black). The flux scale applies to the reference SDSS spectrum and all other spectra are scaled to match the reference spectrum in continuum. In each plot, the error spectra are also shown. The difference spectra for the corresponding epoch together with the associated errors are plotted in the lower panel of each plot. The regions of absorption lines are marked with horizontal lines. The regions of strong telluric absorption are marked by crossed circles.

(MJD 54448). The differences between the IGO and SDSS spectra seen in the top panel of Fig. 4 are mostly a consequence of this. The spectrum contains strong absorption lines from Mg II, Mg I, Mn II, Ni II and Fe II multiplet lines like Fe II λ2586, Fe II λ2382, Fe II λ2344 and excited UV 64. Mn II λ2576 is blended with the Fe II λ2586. The quasar has strong absorption troughs that reach peak depth at $z_{\rm abs} = 0.805$. Like the previous system the absorption trough is resolved into multiple narrow components. Additional Mg II absorption systems are also seen at $z_{\rm abs} = 0.800$ and 0.769. The associated ground-state Fe II lines for these two systems are not detected clearly in our spectrum. As absorption lines are narrow, the continuum can be well defined. So, we measured the total equivalent widths of Mg II, Mg I and the blends near Fe II λ2586 and Fe II λ2382. The results are summarized in Table 2. The quoted error in the equivalent widths also includes uncertainties associated with the continuum placement calculated using repeated continuum fits. This table also confirms the lack of significant (i.e. $>5\sigma$ level) absorption-line variability.

Table 2. Equivalent-width measurements for absorption lines seen towards SDSS J0835+4242.

Spectrum	Equivalent widths (Å)			
	Mg II	Mg I	Fe II λ2586	Fe II λ2382
SDSS	4.1 ± 0.2	0.7 ± 0.2	5.2 ± 0.3	10.7 ± 0.3
IGO-2007	4.5 ± 0.3	0.6 ± 0.2	5.5 ± 0.7	11.5 ± 1.0
IGO-2008	4.5 ± 0.3	0.6 ± 0.2	6.2 ± 0.9	11.4 ± 1.4
IGO-2010	5.6 ± 0.2	0.5 ± 0.2	4.5 ± 0.2	11.2 ± 0.9

We conclude that absorption in SDSS J0835+4242 has not varied significantly over the time period of 4.97 years in the quasar rest frame. The light curve presented in Fig. 1 also suggests that on an average the QSO has not varied in its brightness by more than 0.1 mag.

3.4 SDSS J0840+3633

SDSS J0840+3633 is one among the first known radio loud BAL QSOs (Becker et al. 1997). In the discovery paper, Becker et al. (1997) pointed out the correlation between the column densities of low ionization clouds and radio emissions for three LoBALs and went on to suggest that LoBALs may be transition objects between radio-loud and radio-quiet BAL QSOs. Brotherton et al. (1997) performed the spectropolarimetry of this source and found it to be a highly polarized BAL QSO where the continuum polarization rises steeply towards shorter wavelengths while keeping a constant position angle in the continuum. They considered scattering as the likely polarization mechanism, with the effects of some combination of dust and dilution leading to the wavelength dependences seen. Their studies showed that SDSS J0840+3633 has unpolarized emission lines and increased polarizations in its BAL troughs but complex polarization behaviour across its narrow metastable

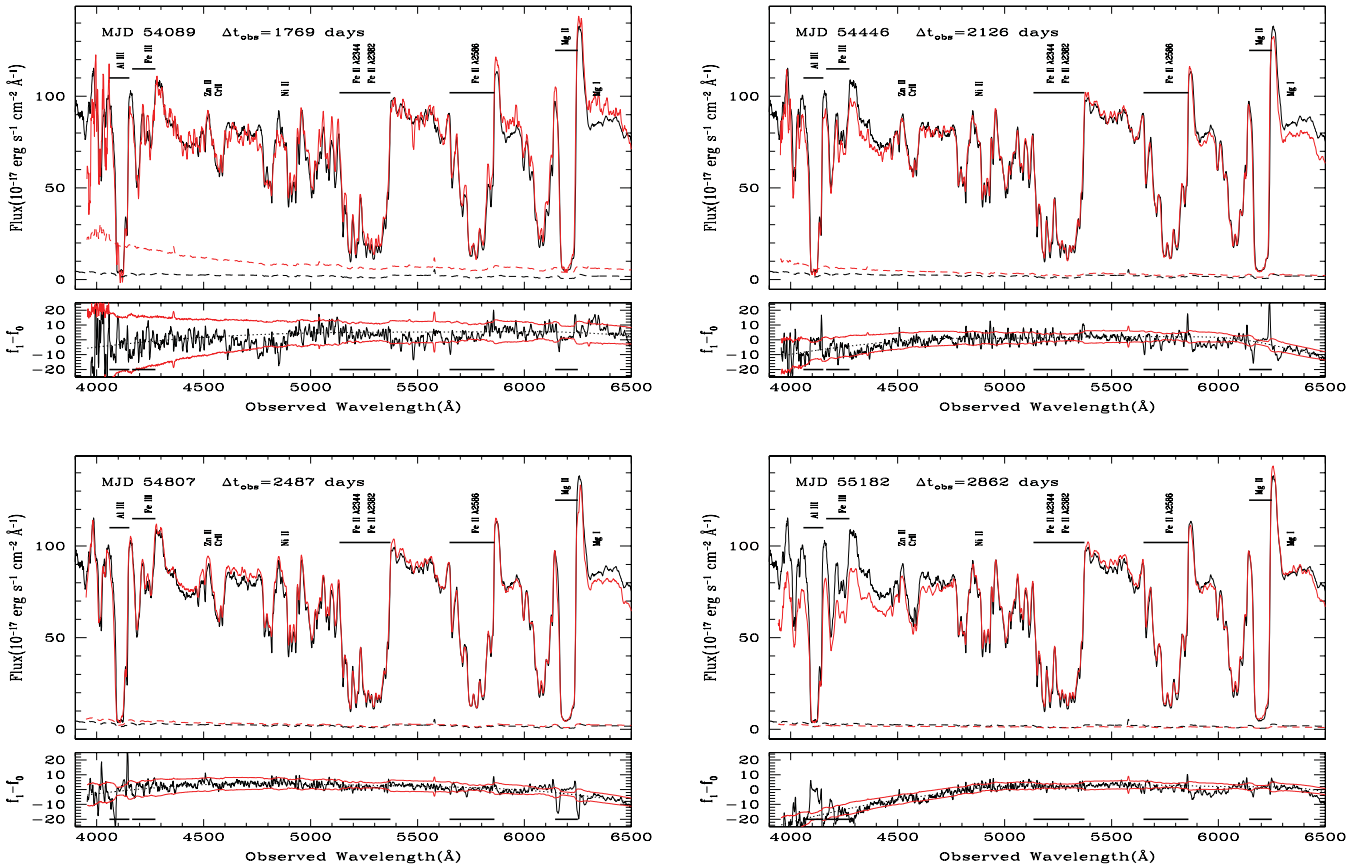

Figure 5. Spectra of SDSS J0840+3633 from IGO (red) epochs are overplotted with the reference SDSS spectra (black). The flux scale applies to the reference SDSS spectrum and all other spectra are scaled to match the reference spectrum in continuum. In each plot the error spectra are also shown. The difference spectra for the corresponding epoch together with the associated errors are plotted in the lower panel of each plot. The regions of absorption lines are marked with horizontal lines. The regions of strong telluric absorption are marked by crossed circles.

troughs. de Kool et al. (2002) studied the KECK/HIRES spectrum of this quasar. Their spectrum reveals outflowing gas with two main components. The physical conditions in the two components are found to be significantly different. This is attributed to the difference of a factor of ∼100 in the distance from the central source. The low-velocity gas has absorption from excited states which indicate low density. Assuming ultraviolet (UV) fluorescence as the possible excitation mechanism, they estimate the distance between the low-velocity absorber and the active nucleus to be ∼230 pc. The high-velocity high-density gas gives rise to strong Fe III and Al III lines. The estimated distance between this gas and the nucleus is ∼1 pc.

Each panel of Fig. 5 shows the IGO spectrum obtained at different epochs overplotted with the reference SDSS spectrum. The spectrum is completely dominated by absorption lines from Mg II, Ni II, Cr II, Al III, Si II, Al II and excited states of Fe II and Fe III. The unabsorbed Mg II emission gives the emission redshift to be 1.230. The BAL troughs are nearly saturated and the continuum is heavily absorbed. The low-velocity Mg II absorption component has a redshift of $z_{\rm abs} = 1.225$ and the troughs extend to a velocity of about 4000 km s^{-1}. Excited states of Fe II comprise UV 63 lines and those of Fe III comprise UV 34 lines.

From the difference spectrum plotted in the lower half of each panel, we see no consistent variations in Mg II, Fe II or Fe III absorption lines. However, the difference spectra have a smooth curvature suggesting a possible difference in the continuum. So, we conclude that the BALs in SDSS J0840+3633 have not varied by an appreciable amount over a rest-frame time period of ∼4 years. From the light curve presented in Fig. 1, we note a gradual increase in the *V* magnitude of the QSO. But the changes are within 0.05 mag. This, together with the strong saturation of the BAL troughs, could be the reason for the lack of line variability.

3.5 SDSS J2215−0045

This is one of the peculiar QSOs identified by Hall et al. (2002) with strong Fe III UV48λ2080, UV34λ1910 and Al III absorption lines in addition to the strong C IV broad absorption line at $z_{\rm abs} \sim 1.36$. Fe II lines are absent and the QSO continuum seems to be dominated by the broad emission from Fe II and Fe III. This is supported by the fact that the QSO continuum does not have strong intrinsic polarization (DiPompeo et al. 2011). The associated Mg II absorption coincides with the 2670 Å break of the Fe emission template; thus, its strength cannot be accurately measured. The three unusual aspects of this QSO are (i) the lack of Fe II absorption while absorption from Fe III fine-structure levels are clearly detected; (ii) the Fe III UV 48 (EP = 5.08 eV) absorption line being stronger than the Fe III UV 34 (EP = 3.73 eV) which is unphysical under local thermodynamic equilibrium (LTE) assumption; and (iii) the emission lines are weak and the redshift of the QSO is determined by a weak and narrow Mg II line at $z_{\rm em} = 1.478$.

In addition to the broad absorption lines discussed above, a narrow associated absorption-line system is detected at redshift $z_{abs} = 1.4752$ based on the presence of Mg II λλ2796, 2803, Fe II λλ2600, 2586, 2382, Si II λ1526 and C II λ1334 in the VLT/UVES data. The Fe II λ 2344 line falls in the red edge of the Na D_1 and D_2 lines from the Galaxy. No absorptions from excited levels like C II* λ1335 or Si II* λ1533 are detected in the spectrum. The VLT/UVES spectrum reveals a second C IV narrow absorption system at a redshift of $z_{abs} = 1.074\,64$. The associated Si IV is beyond the UVES coverage and other associated absorption lines are not detected for this second system. We are unable to confirm these narrow lines in our other data sets due to poor spectral resolution. Hence, we are limited to carry out the time-variability studies for the broad absorption lines only.

Based on photoionization models, de Kool et al. (2002) have shown that the Fe III column density being higher than that of Fe II can be easily produced in a high-density outflow [$\log n_H$ (cm^{-3}) ≥ 10.5 for the ionization parameter $\log U \simeq -2$] with N(H) in a narrow range such that the outflow is constituted only by an Fe III+Al III zone without having the low-ionization zone that usually contains Fe II. Rogerson et al. (2011) have not detected X-ray emission from this source in their *Chandra* observations. They found the logarithm of the ratio between the 2 keV ($l_{2\,keV}$) and 2500 Å ($l_{2500\,Å}$) rest-frame specific luminosities, $\alpha_{ox} \leq -2.45$ and an absorption column of $N(H) \geq 3.4 \times 10^{24}\,cm^{-2}$. They argued that the optical absorption originates from different gas than the one that produces X-ray absorption. Lyman α photons can pump Fe III λ1914 (Johansson et al. 2000). This process may explain the weakness of the UV 34 absorption. On the contrary, due to strong Fe II emission at 1800 Å, and the lack of emission at 2000 Å, the observed spectrum may be consistent with both Fe III UV 48 and UV 34 being saturated with a covering factor of 0.35 (see Hall & Hutsemèkers 2003). From Fig. 1 we see that this is the source with appreciable flux variability in our sample.

While the QSO looks normal in the observed wavelength range ≥6000 Å, there are clear reddening signatures in the blue. As pointed out by Hall et al. (2003), the continuum of this QSO in the wavelength range between 5000 and 9000 Å is dominated by Fe II and Fe III emission. Fig. 6 shows the spectral energy distribution (SED) fitting of SDSS J2215−0045 observed on MJD 51804. We fit the observed spectrum $f(\lambda)$ with the template spectrum $f_t(\lambda)$ using the following parametrization:

$$f(\lambda) = \left[a f_t(\lambda) + b \left(\frac{\lambda}{\lambda_0} \right)^{\alpha} \right] e^{-\tau_\lambda}. \quad (1)$$

We use the χ^2 minimization to get the best values for parameters a, b, α and τ_λ. The second term in the above equation denotes the spectral index differences between the observed and the template

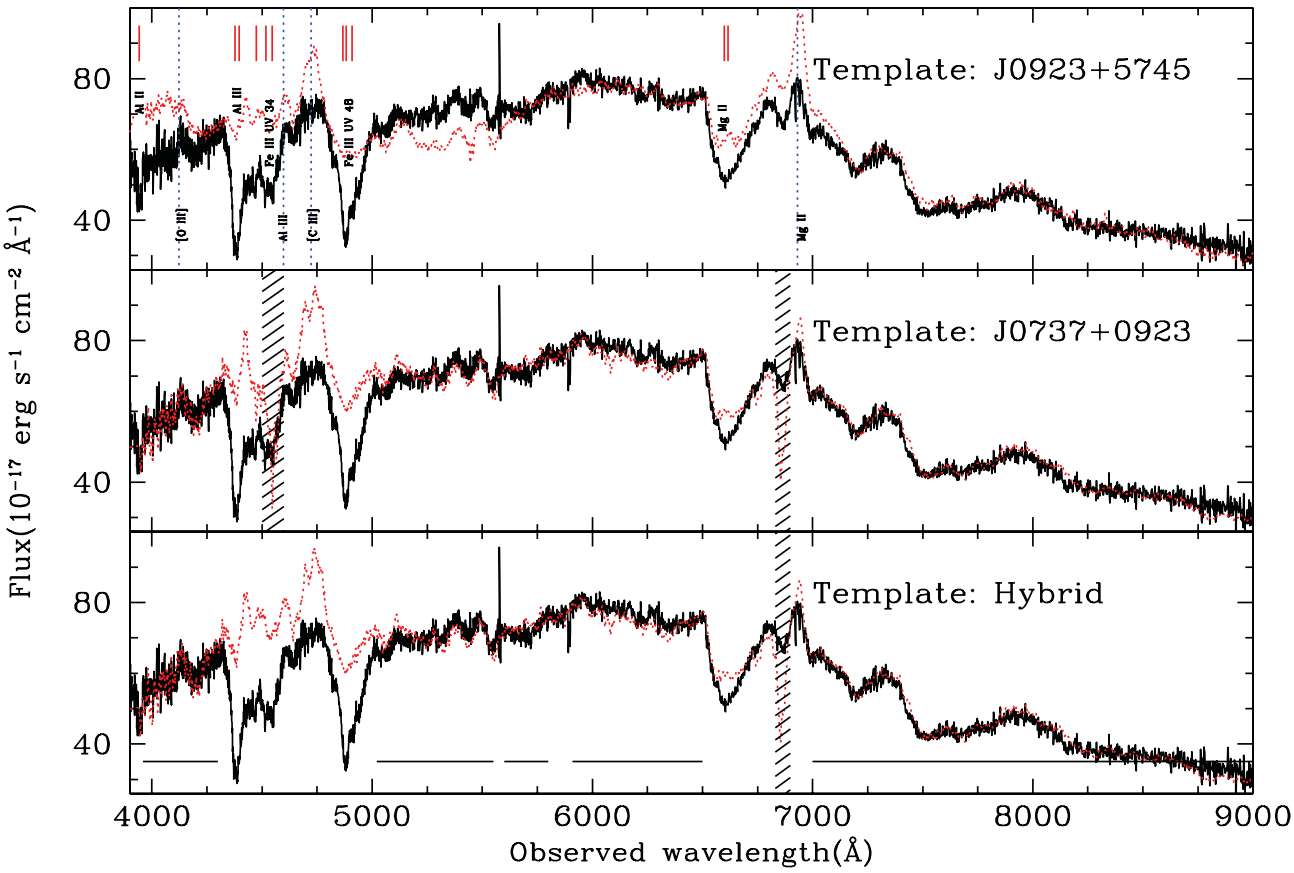

Figure 6. Fitting the SED of SDSS J 2215−0045 observed on MJD 51804. The prominent absorption and emission lines are identified with ticks and dotted lines, respectively. The wavelength bins used for the fitting are shown as horizontal lines in the bottom panel. The top and middle panels show the best-fitting continuum using the spectra of J0923+5745 and J0737+0923 as templates, respectively. The SED is well fitted when we use the spectrum of J0737+0923 as the template. The shaded regions in the middle and bottom panels show the wavelength range affected by absorption in the spectrum of J0737+0923. We use the spectrum of J0923+5745 to reconstruct the SED in these narrow wavelength ranges. A fit to the spectrum of SDSS J2215−0045 using this hybrid template is shown in the bottom panel.

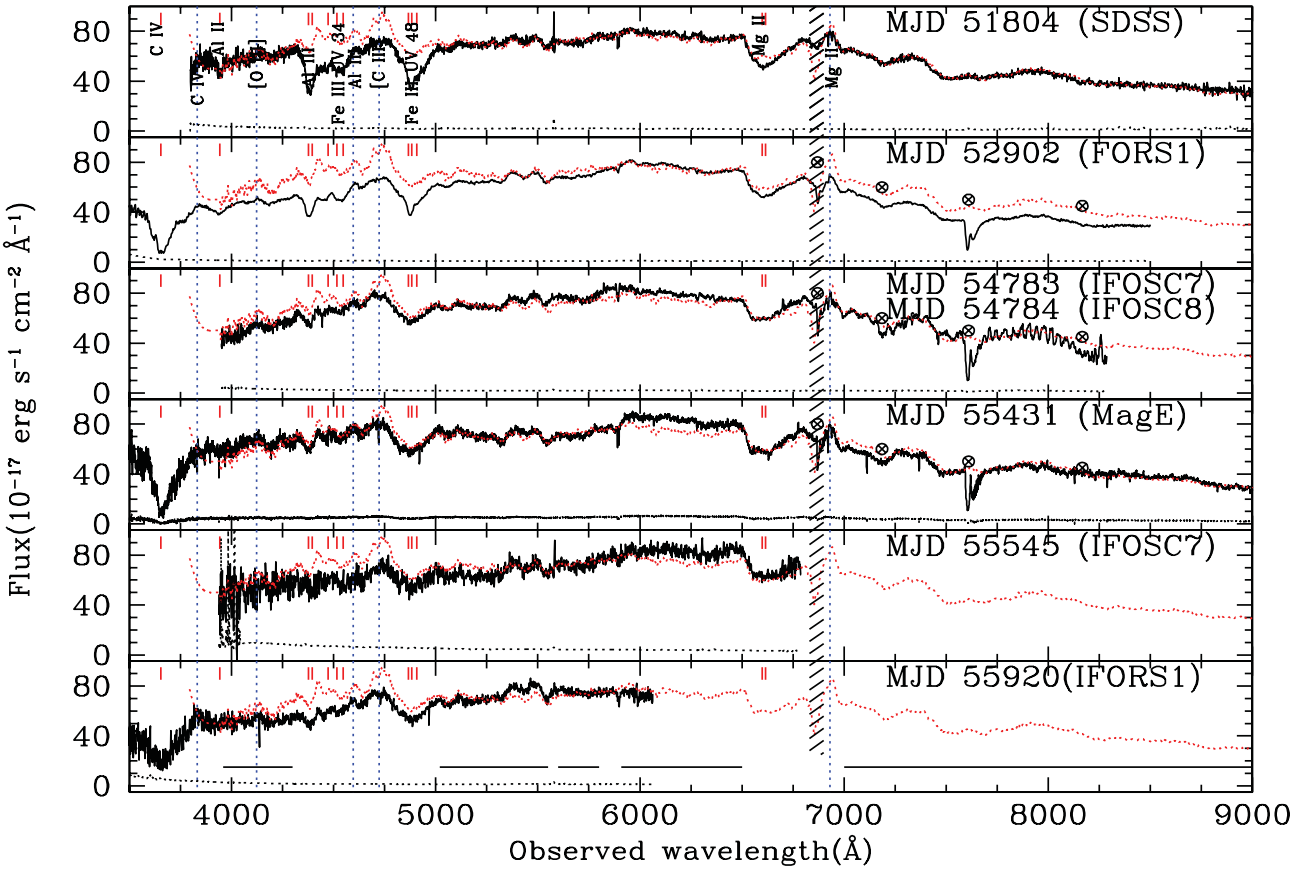

Figure 7. Spectra obtained for SDSS J2215−0045 at different epochs (together with the error spectra) are overplotted with the fit obtained for SDSS using the hybrid template. The prominent absorption and emission lines are identified with ticks and dotted lines, respectively. The wavelength bins used for the fitting are shown as horizontal lines in the bottom panel. Regions of telluric absorption are marked with crossed circles. The shaded regions in all the panels show the wavelength range affected by absorption in the spectrum of J0737+0923.

QSO spectra. The dust optical depth 'τ_λ' is obtained for the Small Magellanic Cloud (SMC) like extinction curve. The fitting method is similar to that described by Srianand et al. (2008). The wavelength ranges used for the fitting are shown as horizontal segments in the top panel. The spectrum has absorption from resonance lines like Mg II, Al II and Al III and fine-structure lines Fe III UV 34 and Fe III UV 48. C IV and Si IV BALs are seen in the VLT/UVES spectrum which has a good coverage in the blue. The position of absorption lines is indicated by vertical marks in Fig. 6. The emission spectrum is illustrated by a dotted line. The top and middle panels show the best-fitting continuum using the spectra of significant iron emitters J0923+5745 and J0737+0923 as templates, respectively. The SED is well fitted when we use the spectrum of J0737+0923 as the template. The shaded regions in the middle and bottom panels show the wavelength range affected by absorption in the spectrum of J0737+0923. We use the spectrum of J0923+5745 to reconstruct the SED in these narrow wavelength ranges. A fit to the spectrum of SDSS J2215−0045 using this hybrid template is shown in the bottom panel. The SED fitting results in an $E(B-V)$ value of −0.083 for the SDSS spectrum. The plot shows that the actual continuum follows the hybrid template reasonably well.

A weak Al II absorption is detected at the redshift of the Al III and Fe III lines. Al III absorption seems very strong. As pointed out by Hall et al. (2002), the Fe III UV 34 blend seems to be weaker than UV 48, if we use a smooth continuum to SDSS J2215−0045. However, it is clear from Fig. 6 that the apparent weakness of UV 34 may be related to the shape of the QSO SED that shows a strong dip at the location of the Fe III UV 48 absorption. The hybrid template used above suggests a stronger [C III] emission line compared to what is observed for SDSS J2215−0045. The removal of this contribution may further reduce the continuum level compared to what is observed for SDSS J2215−0045. Therefore, apparent inconsistencies could be the artefact of the unknown continuum shape and need not be related to the population inversion by some non-equilibrium process. Fig. 7 shows the spectra obtained at different epochs overplotted with the fit obtained for the SDSS data using the hybrid template.

Fig. 8 shows the variability in the absorption lines of SDSS J2215−0045 between the different epoch data. In the top panels, we have overplotted the SDSS, VLT, IGO and MagE data. The plot clearly shows the variations in flux in the region of Al III, Fe III UV 34, Fe III UV 48 and Mg II absorption lines. In order to quantify the optical depth variability in Fig. 8, we plot ratio of spectra between different epochs together with the associated errors. It can be seen that there is significant variability in Mg II, Al III, Fe III UV 34 and Fe III UV 48 absorption lines. The absorption lines have maximum strength in the SDSS spectra. All the later epochs show a decrease in the optical depth with respect to the SDSS data. The lines decreased in optical depth more significantly in the 2008 IGO spectra. However, observations made after 2008 show that both MagE and IGO data are consistent with no variations in the absorption-line optical depths. The Al II absorption is not covered

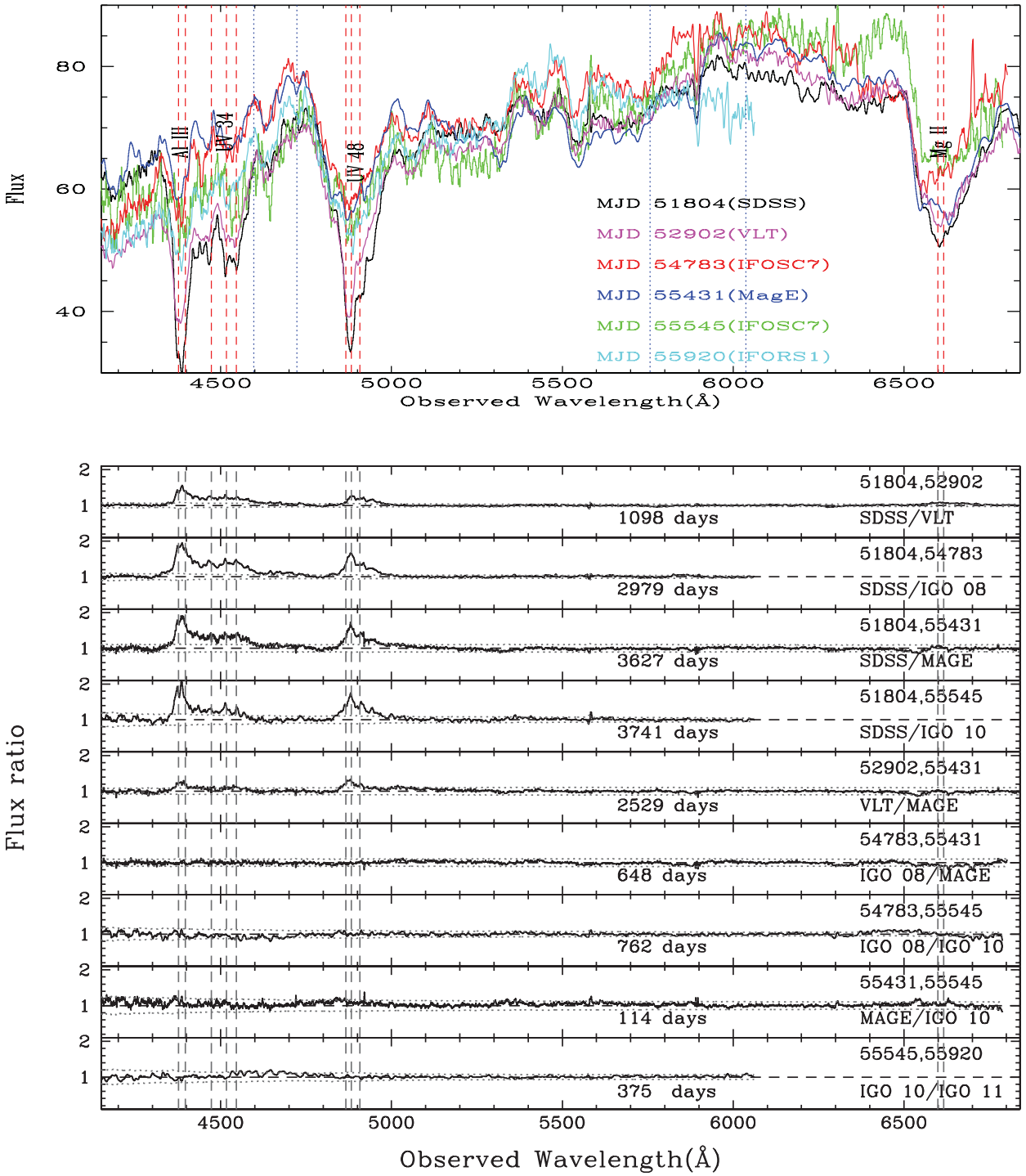

Figure 8. SDSS, VLT, IGO and MagE spectra are plotted and labelled with the observation year in the top panel. The absorption lines are marked with dashed red lines and the emission lines are marked with dotted blue lines. The lower panels show the ratio spectra between different epochs. The epochs of the ratio spectra and the difference between the corresponding MJDs are labelled in each panel.

by our IGO spectra. It is clear from Fig. 7 that at the locations of Al III, Mg II and Fe III UV absorption lines, the observed spectra after 2008 just follow the template. This means that the data are consistent with the disappearance of absorption seen in the SDSS spectrum. We also note that the weak Al II absorption seen in the SDSS spectrum has also disappeared in our MagE spectrum. In Table 3 we give the average ratio measured between different epoch spectra at the wavelength range covered by Fe III UV 34 and 48 lines. If there are no optical depth variation, the average ratio is 1. This table confirms the visual trend seen in Fig. 8.

A strong C IV absorption is detected in the spectra covering $\lambda_{obs} < 4000$ Å. Fig. 9 shows the normalized spectrum in the vicinity of the C IV absorption line which is covered in the VLT/FORS1, VLT/UVES, MagE and the IGO/FORS1 data. As C IV falls in a region which is free of Fe emission, we fitted a low-order polynomial connecting the absorption-free regions close to the C IV line for

Table 3. Average flux ratios in the region of absorption lines for SDSS J2215−0045.

Epoch 1	Epoch 2	Δt^a (days)	Average ratio Fe III[b] UV 34 (Å)	Fe III[c] UV 48 (Å)
SDSS	VLT-FORS1	1098	1.14 ± 0.04	1.09 ± 0.06
SDSS	IGO-2008	2979	1.27 ± 0.04	1.20 ± 0.06
SDSS	MagE	3627	1.23 ± 0.04	1.20 ± 0.06
SDSS	IGO-2010	3741	1.17 ± 0.04	1.23 ± 0.06
VLT-FORS1	MagE	2529	1.04 ± 0.06	1.10 ± 0.09
IGO-2008	MagE	648	0.99 ± 0.04	0.99 ± 0.06
IGO-2008	IGO-2010	762	0.94 ± 0.04	1.00 ± 0.06
MagE	IGO-2010	114	1.03 ± 0.02	1.07 ± 0.03
IGO-2010	IGO-2011	375	1.05 ± 0.04	1.00 ± 0.06

[a]Elapsed time in observers frame; [b]over the observed wavelength range 4316–4762 Å; [c]over the observed wavelength range 4809–5024 Å.

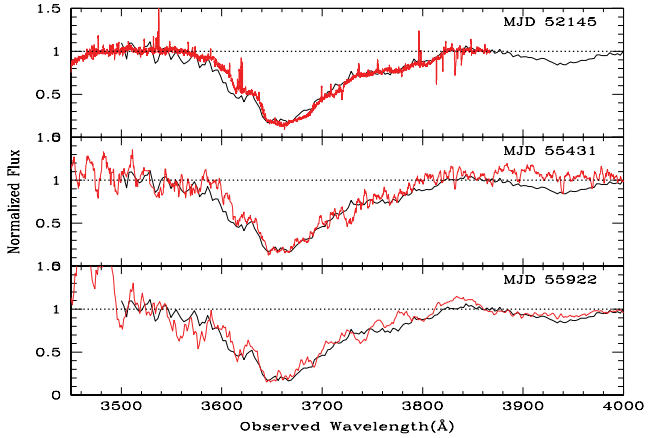

Figure 9. Normalized C IV absorption line, seen in VLT/UVES, MagE and IGO/IFORS1 (in red/grey) spectra, is compared to the VLT/FORS1 spectra obtained on MJD 52902 (black). In all these cases the continuum normalization is done using lower order polynomials connecting the absorption-free regions on either side of the C IV absorption.

continuum normalization. We note the C IV absorption is much broader than that of Al III (or Al II). This suggests that the two species may originate from two different regions (i.e. two distinct components of a co-spatial multiphase structure or from gas at distinctly different locations). The Si IV line falls at the edge of the MagE spectrum and is not covered by VLT/FORS1. From the figure, it can be seen that C IV has not changed significantly as the low ionization lines. Note that the C IV line does not become zero. This could mean either that C IV is optically thin or that the absorbing gas does not cover the background source.

In the following section, we discuss the implications of the observed variability in this source.

4 DISCUSSION ON VARIABILITY IN SDSS J2215−0045

Variability in broad absorption lines has several origins. The simplest explanations are (1) change in the ionizing condition, (2) proper motion of absorbing clouds (Ma 2002; Hamann et al. 2008; Leighly et al. 2009; Krongold, Binette & Hernández-Ibarra 2010; Rodríguez Hidalgo, Hamann & Hall 2011; Vivek et al. 2012) and (3) covering factor variability of the absorbing gas (see e.g. Srianand & Shankaranarayanan 1999).

In the case of SDSS J2215−0045, the variability in the Al III and Fe III fine-structure lines is unambiguously established. As we do not have direct access to the column density of the Fe III ground-state absorption, it will be difficult to draw any conclusion on the variations of the relative population of the excited level with respect to the ground level. However, we know that in the case of photoionization models, Fe III will closely trace Al III. Also, the weakness of Al II and the lack of Fe II absorption are consistent with the range in the ionization parameter being very narrow (see discussion on this by de Kool et al. 2002). Thus, any small change in the ionizing radiation will change both Al III and Fe III column densities rapidly. A simple ionization change (even without changing the excitation temperature) will change the column density of Fe III fine-structure levels. As discussed in Sections 2, the light curve of SDSS J2215−0045 is consistent with the V-band photometric variability of > 0.2 mag. The actual variability in the UV range that controls the ionization state of the gas can be higher. From figs 6 and 7 of de Kool et al. (2002), it is apparent that the ion fraction of Fe III (and Al III) can be significantly reduced even for a small change in the ionization parameter. Compared to the SDSS epoch, our IGO data were taken when the QSO was 0.5 mag brighter. Therefore, the observed variability of the Fe III and Al III lines is consistent with the photoionization-induced variability.

The smallest time-scale over which we have seen the variation is between the SDSS in 2000 and VLT in 2003. This time period corresponds to a time-scale of ∼1.211 years in the quasar rest frame. The variability time-scale can be used to constrain the electron density of the absorbing gas.

For a moderately ionized gas $n_i > n_{i+1}$, the recombination time-scale can be approximated to (see Srianand & Petitjean 2001)

$$t_r = (n_e \alpha_r)^{-1}. \quad (2)$$

The variability time-scale gives the recombination time-scale, if the variations are assumed to be caused due to changes in the optical depth. Using the recombination cross-section for Al III given by the CHIANTI atomic data base (Dere et al. 1997, 2009), the lower limit on the electron density, n_e, is given by

$$n_e \geq 1.3214 \times 10^4 t_{yr}^{-1}, \quad (3)$$

where t_{yr} is the elapsed time in years. The recombination coefficients are calculated for a temperature of 10 000 K. Putting $t_{yr} = 1.211$ in the above equation results in an electron density of $n_e \geq 1.091 \times 10^4$ cm^{-3}. This is coincident with but not as high as what has been suggested by the models of de Kool et al. (2002). However, the lack of variability in C IV under this scenario could mean that the absorbing gas has multiphase structure with C IV and Fe III absorption originating from different phases.

Models of FeLoBALs by Faucher-Giguère et al. (2012) suggest the in situ formation of Fe BALs in the ISM of host galaxies by shocks induced by the QSO blast wave. Going along this line, Rogerson et al. (2011) put forward a model where an accelerating, relatively low-density wind collides with dense Fe III clumps and produces the observed absorption lines. Since Fe III clumps are ablated in this process, the Fe III troughs will decrease with time unless the wind encounters new clumps. The variability seen in the present system is consistent with this scenario. In this case, Fe III absorption is produced from a distinct region (probably the ISM of the host galaxy) compared to that of C IV. However, as this time-scale should be shorter than the sound-crossing time for a $T \sim 10^4$ K gas, we can

write the cloud thickness as

$$\Delta R = \frac{0.01 \times t_{\rm yr}}{640}\,{\rm pc} = 6 \times 10^{13}\,{\rm cm}. \quad (4)$$

This is much smaller than the size of the UV continuum emitting region. This thickness is much less than what one gets from photoionization models.

Recently, several cases of emergence and subsequent disappearance of new components have been reported in the literature (Ma 2002; Hamann et al. 2008; Leighly et al. 2009; Krongold et al. 2010; Rodríguez Hidalgo et al. 2011; Vivek et al. 2012). In all these cases, the absorbing gas transiting perpendicular to our line of sight is considered as a viable explanation. Such an explanation can also hold for the present case.

To investigate this scenario, we derive some basic parameters for SDSS J2215−0045. The SDSS u and g magnitudes are converted into the B magnitude following the transformation equation of Jester et al. (2005) obtained for $z \leq 2.1$ QSOs. We get the bolometric luminosity for this source from the B magnitude as 2.7×10^{47} erg s^{-1} using the prescription of Marconi et al. (2004). The bolometric luminosity corresponds to a black hole mass of $2.2 \times 10^9\,{\rm M}_\odot$. The diameter of the disc within which 90 per cent of the 2700 Å continuum is emitted is obtained as 1.49×10^{16} cm (∼46 times the Schwarzschild radius) as expected in a Shakura & Sunyaev thin accretion disc model (Hall et al. 2011). Variability in SDSS J2215−0045 has occurred between the SDSS and IGO observations. If we take the number of days elapsed between the SDSS and IGO observations (3740 d in observer's frame or 1509 d in quasar frame) as an upper limit on the transit time of the gas, the transverse velocity of the gas can be estimated as $v_\perp \geq 1140\,{\rm km\,s^{-1}}$ if we assume the projected size of the gas to be much smaller than the emitting region and a face-on disc. Based on the redshift of the Al III absorption, we infer the line-of-sight velocity to be of the order of 15 000 km s^{-1}. Therefore, like in the case of J1333+0012 (Vivek et al. 2012), the outflow should be very close to the line of sight such that the transverse velocity is much smaller than the line-of-sight velocity.

5 RESULTS AND DISCUSSION

We present the results of a spectroscopic monitoring of five FeLoBALs for a period of 10 years. We also present the photometric light curves of all these sources obtained from CRTS.

In one of these QSOs, SDSS J2215−0045, we detected the absorption-line variability of the Al III and Fe III fine-structure lines. However, there is no clear variation in the absorption profile of the C IV absorption. Our results are consistent with low ions and C IV originating from different components along the line of sight. The absorption-line variability could be related to changes in the ionization state of the gas and/or to changes in the covering factor due to transverse motion of the gas. The light curve of SDSS J2215−0045 suggests brightening of this QSO when the absorption line became weak. This together with the expected narrow range in the allowed parameters of the photoionization models (de Kool et al. 2002; Rogerson et al. 2011) means that the observed variability can very well be explained by changes in the photoionization rates. The data are also consistent with the models of Rogerson et al. (2011) in which a shock-heated cloud that produces Fe III absorption being ablated producing strong variations in the absorption strength. Regular photometric and spectroscopic monitoring of this source is needed to distinguish between these alternatives.

In the remaining cases, no significant variation in the absorption line is detected. As these sources do not show any strong flux variability, photoionization-induced absorption-line variability is not expected in these sources. However, if the low ion absorption in these systems is due to the ISM (or high-density clump far away from the central QSO) being shock heated by the QSO feedback, then we do not find any evidence of this gas being ablated with time. Also, we can conclude that either the projected extent of the gas is larger than the continuum emitting region or the transverse velocity is small.

If FeLoBALs are a different set of population (where the absorption occurs far away from the central engine), then comparing the occurrence of variability in these objects with those of HiBALs and LoBALs without fine-structure lines will throw light on the nature of the BAL phenomenon in QSOs.

ACKNOWLEDGMENTS

We wish to acknowledge the IUCAA/IGO staff for their support during our observations and Maria-Jose Maureira for help with MagE observations. We also thank Dr DiPompeo for sharing VLT/FORS data with us and the anonymous referee for useful suggestions. MV gratefully acknowledges the University Grants Commission, India, for financial support through the RFSMS scheme and IUCAA for hospitality, where most of this work was done. RS and PP gratefully acknowledge support from the Indo-French Centre for the Promotion of Advanced Research (Centre Franco-Indien pour la promotion de la recherche avancée) under Project N.4304-2.

REFERENCES

Allen J. T., Hewett P. C., Maddox N., Richards G. T., Belokurov V., 2011, MNRAS, 410, 860
Barlow T. A., Junkkarinen V. T., Burbidge E. M., 1989, ApJ, 347, 674
Barlow T. A., Junkkarinen V. T., Burbidge E. M., Weymann R. J., Morris S. L., Korista K. T., 1992, ApJ, 397, 81
Bautista M. A., Dunn J. P., Arav N., Korista K. T., Moe M., Benn C., 2010, ApJ, 713, 25
Becker R. H., Gregg M. D., Hook I. M., McMahon R. G., White R. L., Helfand D. J., 1997, ApJ, 479, L93
Bochanski J. J. et al., 2009, PASP, 121, 1409
Brotherton M. S., Tran H. D., van Breugel W., Dey A., Antonucci R., 1997, ApJ, 487, L113
Capellupo D. M., Hamann F., Shields J. C., Rodríguez Hidalgo P., Barlow T. A., 2011, MNRAS, 413, 908
Dai X., Shankar F., Sivakoff G. R., 2008, ApJ, 672, 108
de Kool M., Becker R. H., Arav N., Gregg M. D., White R. L., 2002, ApJ, 570, 514
Dere K. P., Landi E., Mason H. E., Monsignori Fossi B. C., Young P. R., 1997, A&AS, 125, 149
Dere K. P., Landi E., Young P. R., Del Zanna G., Landini M., Mason H. E., 2009, A&A, 498, 915
DiPompeo M. A., Brotherton M. S., De Breuck C., 2011, ApJS, 193, 9
Drake A. J. et al., 2009, ApJ, 696, 870
Dunn J. P. et al., 2010, ApJ, 709, 611
Farrah D., Lacy M., Priddey R., Borys C., Afonso J., 2007, ApJ, 662, L59
Faucher-Giguère C.-A., Quataert E., Murray N., 2012, MNRAS, 420, 1347
Foltz C. B., Weymann R. J., Morris S. L., Turnshek D. A., 1987, ApJ, 317, 450
Gibson R. R., Brandt W. N., Schneider D. P., Gallagher S. C., 2008, ApJ, 675, 985
Gibson R. R., Brandt W. N., Gallagher S. C., Hewett P. C., Schneider D. P., 2010, ApJ, 713, 220
Green P. J., Aldcroft T. L., Mathur S., Wilkes B. J., Elvis M., 2001, ApJ, 558, 109
Hall P. B., Hutsemèkers D., 2003, in Collin S., Combes F., Shlosman I., eds, ASP Conf. Ser. Vol. 290, Active Galactic Nuclei: From Central Engine to Host Galaxy. Astron. Soc. Pac., San Francisco, p. 209

Hall P. B. et al., 2002, ApJS, 141, 267
Hall P. B., Hutsemékers D., Anderson S. F., Brinkmann J., Fan X., Schneider D. P., York D. G., 2003, ApJ, 593, 189
Hall P. B., Anosov K., White R. L., Brandt W. N., Gregg M. D., Gibson R. R., Becker R. H., Schneider D. P., 2011, MNRAS, 411, 2653
Hamann F., Kaplan K. F., Rodríguez Hidalgo P., Prochaska J. X., Herbert-Fort S., 2008, MNRAS, 391, L39
Hewett P. C., Foltz C. B., 2003, AJ, 125, 1784
Jester S. et al., 2005, AJ, 130, 873
Johansson S., Zethson T., Hartman H., Ekberg J. O., Ishibashi K., Davidson K., Gull T., 2000, A&A, 361, 977
Korista K. T., Bautista M. A., Arav N., Moe M., Costantini E., Benn C., 2008, ApJ, 688, 108
Krongold Y., Binette L., Hernández Ibarra F., 2010, ApJ, 724, L203
Leighly K. M., Hamann F., Casebeer D. A., Grupe D., 2009, ApJ, 701, 176
Lundgren B. F., Wilhite B. C., Brunner R. J., Hall P. B., Schneider D. P., York D. G., Vanden Berk D. E., Brinkmann J., 2007, ApJ, 656, 73
Ma F., 2002, MNRAS, 335, L99
Marconi A., Risaliti G., Gilli R., Hunt L. K., Maiolino R., Salvati M., 2004, MNRAS, 351, 169
Moe M., Arav N., Bautista M. A., Korista K. T., 2009, ApJ, 706, 525
Murray N., Chiang J., 1995, ApJ, 454, L105
Reichard T. A. et al., 2003, AJ, 125, 1711
Rodríguez Hidalgo P., Hamann F., Hall P., 2011, MNRAS, 411, 247
Rogerson J. A., Hall P. B., Snedden S. A., Brotherton M. S., Anderson S. F., 2011, New Astron., 16, 128
Smith L. J., Penston M. V., 1988, MNRAS, 235, 551
Srianand R., Petitjean P., 2001, A&A, 373, 816
Srianand R., Shankaranarayanan S., 1999, ApJ, 518, 672
Srianand R., Gupta N., Petitjean P., Noterdaeme P., Saikia D. J., 2008, MNRAS, 391, L69
Stalin C. S., Srianand R., Petitjean P., 2011, MNRAS, 413, 1013
Trump J. R. et al., 2006, ApJS, 165, 1
Turnshek D. A., Grillmair C. J., Foltz C. B., Weymann R. J., 1988, ApJ, 325, 651
Vivek M., Srianand R., Mahabal A., Kuriakose V. C., 2012, MNRAS, 421, L107
Voit G. M., Weymann R. J., Korista K. T., 1993, ApJ, 413, 95
Wampler E. J., Chugai N. N., Petitjean P., 1995, ApJ, 443, 586

This paper has been typeset from a TEX/LATEX file prepared by the author.